J. Fluid Mech. (2020), vol. 890, A7. © The Author(s), 2020. Published by Cambridge University Press doi:10.1017/jfm.2020.127

890 A7-1

On the origins of transverse jet shear layer instability transition

Takeshi Shoji¹, Elijah W. Harris¹, Andrea Besnard¹, Stephen G. Schein¹ and Ann R. Karagozian¹,†

¹Department of Mechanical and Aerospace Engineering, University of California Los Angeles, Los Angeles, CA 90095-1597, USA

(Received 30 October 2019; revised 30 January 2020; accepted 5 February 2020)

This experimental study explores the physical mechanisms by which a transverse jet's upstream shear layer can transition from being a convective instability to an absolute/global instability as the jet-to-cross-flow momentum flux ratio J is reduced. As first proposed in computational studies by Iyer & Mahesh (J. Fluid Mech., vol. 790, 2016, pp. 275–307), the upstream shear layer just beyond the jet injection may be analogous to a local counter-current shear layer, which is known for a planar geometry to become absolutely unstable at a large enough counter-current shear layer velocity ratio, R_1 . The present study explores this analogy for a range of transverse jet momentum flux ratios and jet-to-cross-flow density ratios S, for jets containing differing species concentrations (nitrogen, helium and acetone vapour) at several different jet Reynolds numbers. These studies make use of experimental data extracted from stereo particle image velocimetry as well as simultaneous stereo particle image velocimetry and acetone planar laser-induced fluorescence imaging. They provide experimental evidence for the relevance of the counter-current shear layer analogy to upstream shear layer instability transition in a nozzle-generated transverse jet.

Key words: absolute/convective instability, jets, shear layers

1. Introduction

A jet in cross-flow (JICF) or transverse jet typically consists of a round jet issuing perpendicularly into cross-flow. This canonical three-dimensional flow field has been studied for many decades, in part because of its extensive applications to engineering propulsion systems (Karagozian 2010). The interaction between the jet and cross-flow generates diverse vortical structures, including the well-known counter-rotating vortex pair (CVP), shown schematically in figure 1(a). The jet-to-cross-flow density ratio, $S \equiv \rho_j/\rho_{\infty}$, velocity ratio, $R \equiv U_j/U_{\infty}$, and momentum flux ratio, $J \equiv \rho_j U_j^2/\rho_{\infty} U_{\infty}^2$, are among the non-dimensional parameters often used in studying JICF behaviour, in addition to the jet Reynolds number, $Re_j \equiv \rho_j U_j D/\mu_j$, which is based on the mean jet exit velocity U_i , jet diameter D and the absolute viscosity of the jet fluid, μ_i .

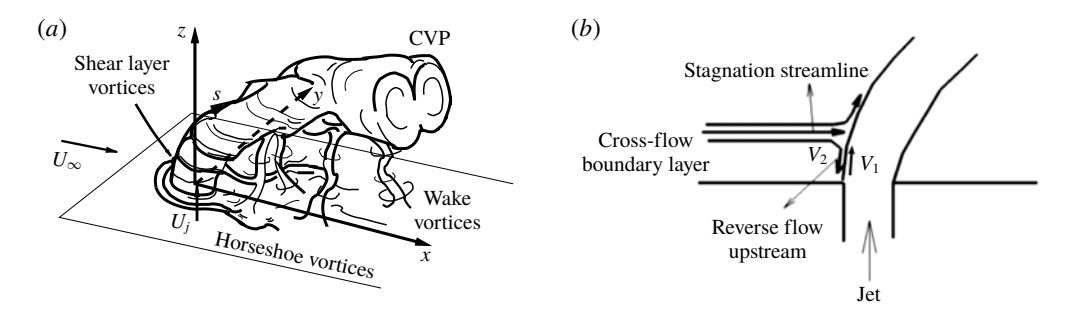


FIGURE 1. (a) Schematic of a flush-injected JICF, including orientation of coordinate axes x, y, z, and jet USL trajectory s (adapted from Fric & Roshko (1994)). (b) Schematic of the effect of jet blockage of cross-flow, creating local negative velocity V_2 upstream of the USL adjacent to a positive vertical velocity V_1 within the jet (adapted from Iyer & Mahesh (2016)).

A Strouhal number $St_o \equiv f_o D/U_j$ non-dimensionalizes frequencies associated with the fundamental upstream shear layer (USL) instability corresponding to initial vortex rollup (Getsinger *et al.* 2014). Alternative length scales that can be used in the definition of Strouhal number include momentum thicknesses for the jet fluid as well as the USL; this scaling will be discussed later in detail.

The transverse jet's USL is known to transition from being convectively unstable at larger J values to being absolutely or globally unstable at smaller J. There is extensive experimental evidence for this transition, for both equidensity (Megerian et al. 2007; Davitian et al. 2010) and low-density (Getsinger, Hendrickson & Karagozian 2012) jets in cross-flow. For the equidensity JICF in which nitrogen is injected from a nozzle that is flush with respect to the injection wall into a cross-flow of air, at both $Re_i = 2000$ and 3000, hot-wire-based studies determine that the USL transition from convective to absolute instability occurs when increasing cross-flow velocity causes the jet-to-cross-flow velocity ratio to fall below a critical value of $R \approx 3.1$. For low-density transverse jets consisting of mixtures of nitrogen and helium injected into air from a flush nozzle, the transition to absolute instability is documented in Getsinger et al. (2012) to occur for momentum flux ratio $J \lesssim 10$ and/or density ratio $S \lesssim 0.40$, the latter of which is consistent with low-density free-jet studies in this Reynolds-number regime (Hallberg & Strykowski 2006). At these relatively low R or J values, the transverse jet can be deflected considerably by the cross-flow, causing a slowly varying parallel flow approximation, which works well in a local linear stability analysis (LSA) of the flow for J > 10 (Alves, Kelly & Karagozian 2007, 2008), to be less appropriate for the USL. Global LSA for the JICF at lower velocity or momentum flux ratios (e.g. J < 10), however, has shown success in demonstrating sustained self-excited global oscillations in the deflected transverse jet's USL (Bagheri et al. 2009; Peplinski, Schlatter & Henningson 2015; Regan & Mahesh 2017).

Direct numerical simulations (DNS) by Iyer & Mahesh (2016) for the equidensity JICF using the same flush nozzle geometry as in the experiments of Megerian *et al.* (2007), for the cases R = 4 and 2 at $Re_j = 2000$, show remarkably good qualitative and quantitative agreement in predicted spectral characteristics (e.g. St_o values) for the jets based on vertical velocity disturbances along the USL. Additional experimental studies utilizing a flush round pipe for the equidensity JICF (Getsinger *et al.* 2014) demonstrate a transition to absolute/global instability in the jet's USL for $J \lesssim 10$,

also observed in DNS (Bagheri et al. 2009), although convective instabilities at higher J values in the experiments are considerably weaker than for flush nozzle-injected jets. Further experiments involving optical diagnostics enable detailed study of the relationships among JICF shear layer instabilities, flow structure, molecular mixing and dynamical characteristics (Getsinger et al. 2014; Gevorkyan et al. 2016, 2018).

Computations by Iyer & Mahesh (2016) also investigate the similarity in the JICF USL instability transition to that of a two-dimensional (2-D) counter-current shear layer (CCSL), where the signs of the velocities of the two streams oppose one another. As indicated schematically in figure 1(b), cross-flow blockage by the jet can create a stagnation streamline and reverse flow region just outside of the USL near injection, creating a negative velocity $V_2 < 0$ analogous to that in a CCSL, contrasting a positive vertical flow within the jet, $V_1 > 0$. The stagnation streamline generally appears well outside of the cross-flow wall boundary layer, even at large velocity ratios (Megerian et al. 2007). In general a CCSL may be characterized by a mixing or shear layer ratio R_1 based on the velocities V_1 and V_2 shown in figure 1(b),

$$R_1 = \frac{V_1 - V_2}{V_1 + V_2},\tag{1.1}$$

so that $R_1 > 1.0$ denotes counter-flow and $R_1 < 1.0$ denotes co-flow. Inviscid spatio-temporal stability analysis of an incompressible, planar CCSL using a hyperbolic tangent velocity profile (Huerre & Monkewitz 1985) indicates that the CCSL becomes absolutely unstable when R_1 exceeds a critical value, $R_{1,cr} = 1.315$. Corresponding experiments for an axisymmetric (round) jet with a finite region of exterior suction (Strykowski & Niccum 1991) suggest a critical velocity ratio very close to the theoretical value, $R_{1,cr} \approx 1.32$. Similar inviscid LSA for the compressible planar CCSL, with streams of differing densities, has also been performed (Pavithran & Redekopp 1989), employing the Crocco-Busemann relation and an equation of state for a perfect gas. Corresponding axisymmetric counter-current jet experiments by Strykowski & Niccum (1992) quantify values of $R_{1,cr}$ for various density ratios S. For the equidensity round transverse jet, Iyer & Mahesh (2016) utilize DNS-generated velocity fields in the USL to compute the effective shear layer ratio R_1 just downstream of jet injection. In the R=4 case, R_1 is estimated in the centre plane (y = 0 plane) to be 1.2, while for the R = 2 simulation, $R_1 = 1.44$. Even with the simplified parallel flow approximation for the JICF at the low velocity ratio, the findings suggest that these two different JICF flow conditions could straddle the transition between convective and absolute instability when viewed in the context of a local CCSL occurring at the upstream edge of flush JICF injection. Despite the relatively limited extent of both the negative and positive velocity regions for the flush nozzle-generated JICF, the CCSL model appears to be consistent with instability differences for these two transverse jet cases.

The compelling nature of this analogy for transition in the transverse jet's shear layer instabilities, coupled with recent observations on differences in the transition conditions based on fluid species present in the jet, has motivated the present examination. Data from a rather wide range of experimental flow conditions can be used in exploring the analogy as a means of exploring the nature of the transition and understanding the physics of its origins.

2. Experimental configuration

This experimental study on gaseous jets in cross-flow utilized a low-velocity wind tunnel with hot-wire anemometry for spectral characterization and laser diagnostics

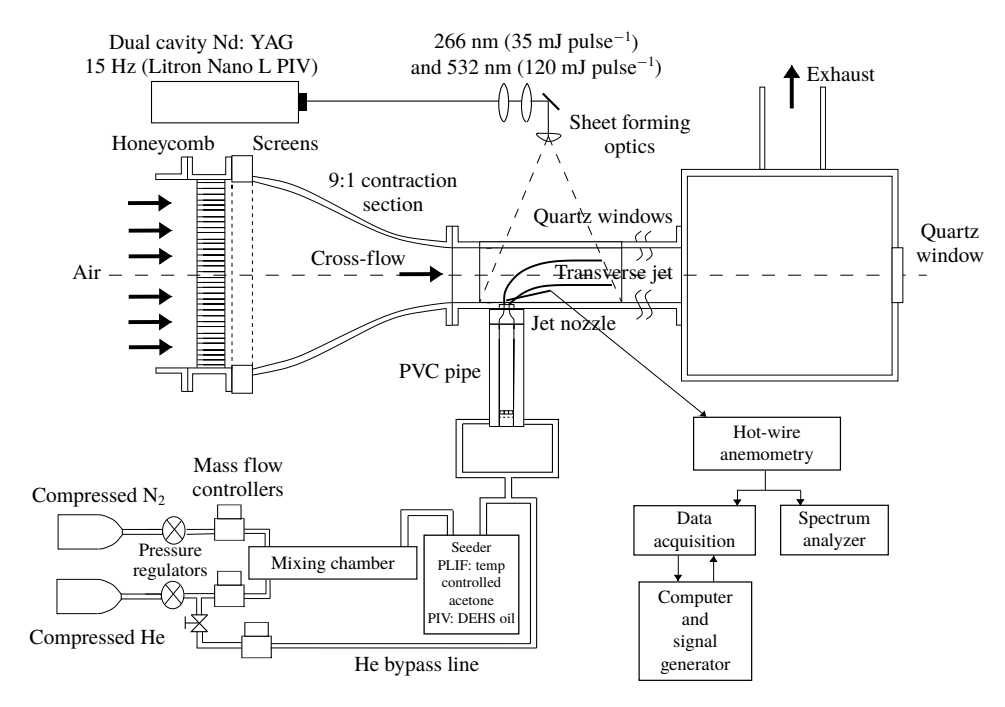


FIGURE 2. Low-velocity wind tunnel with associated hot-wire anemometry and optical diagnostic apparatus. One additional tunnel section, of identical dimensions, was situated downstream of the test section shown.

for scalar and velocity field quantification. The experimental configuration is shown in figure 2. Details on the set-up and optical diagnostics are available in recent papers (Getsinger *et al.* 2014; Gevorkyan *et al.* 2016, 2018), but a brief overview is provided here. A cross-flow of air in the downstream (positive x) direction was created by a centrifugal blower placed upstream of the test section, which had dimensions $30 \text{ cm} \times 12 \text{ cm} \times 12 \text{ cm}$. The turbulence intensity in the tunnel-generated cross-flow in the absence of the jet was less than 1.5% of the maximum achievable cross-flow velocity of approximately 7 m s^{-1} . A Plexiglas window fitted into the side of the test section enabled optical access for laser diagnostics in the centre plane (y = 0 or x - z plane in figure 1a).

This study primarily utilized jets issuing perpendicularly into cross-flow from a fifth-order polynomial nozzle with a 64:1 area ratio contraction, mounted flush to the bottom floor of the test section and with an exit diameter D=4.04 mm (referenced as the 'flush nozzle'). For one dataset, a fifth-order polynomial nozzle with the same contraction ratio and D=7.59 mm (the 'larger flush nozzle') was examined. Each created a top-hat-like velocity profile with a thin jet boundary layer in the absence of cross-flow (e.g. as documented in Megerian *et al.* (2007)). The jet fluid comprised mixtures of helium and nitrogen and, for cases involving laser diagnostics, tracer species. For optical diagnostics, the jet fluid flowed into a temperature-controlled acetone seeder for planar laser-induced fluorescence (PLIF) imaging of the acetone, which was maintained in the vapour phase, and/or into a particle seeder for stereo particle image velocimetry (PIV) measurements. The jet Reynolds number could be fixed, while density ratios were varied in the range $0.35 \le S \le 1.00$. Adjusting the mole fractions of various species enabled the desired densities and jet Reynolds

numbers to be achieved (Gevorkyan *et al.* 2016, 2018). Jet density and viscosity were calculated considering all constituents in the jet, with or without inclusion of the acetone mole fraction ψ , depending on experimental conditions. The viscosity of the jet was determined by the Wilke formulation without acetone vapour in the jet (Bird, Stewart & Lightfoot 1960) and by the Reichenberg method with acetone (Poling, Prausnitz & O'Connell 2001). The desired momentum flux ratio was achieved by varying the cross-flow velocity U_{∞} for fixed S and Re_j ; the present studies focused on the range $3 \le J \le 61$. As per the analysis in Canzonieri (2009), the maximum experimental uncertainty in jet density was 1.5% in the absence of acetone. With acetone present, the additional sources of error associated with the pressure and temperature control for the acetone seeder produced a maximum uncertainty of 5.1% in jet density (Shoji 2017).

These experiments utilized constant-temperature hot-wire anemometry (Dantec 55P15), either with or without acetone vapour seeded in the jet, enabling spectral measurements of the transverse jet's USL to be made. A single-component, boundarylayer-type hot-wire probe was used with a triple-axis linearly staged platform to control position to within 1 µm accuracy. Spectral data were fed to a dual-channel dynamic signal analyser (HP Model 35665A) and averaged over 40 instantaneous frequency distributions. The spectral measurements were applied over a 6.4 kHz range with 8 Hz resolution. Separately, stereo PIV measurements were utilized in the jet centre plane to acquire velocity fields in a non-intrusive manner. Besides PIV-only data, velocity data were acquired via the PIV portion of simultaneous stereo PIV and acetone PLIF imaging. A dual-cavity Q-switched Nd:YAG laser (Litron Nano L PIV) was employed in most of the studies with second- and fourth-harmonic generators to generate concentric 532 nm and 266 nm wavelength light for PIV and PLIF imaging, respectively. Each cavity was able to produce a 8 ns full width at half-maximum (FWHM) pulse, with 30 mJ at 266 nm and 120 mJ at 532 nm, at a maximum repetition rate of 15 Hz, although the repetition rate used in actual measurements was typically 1 Hz, as discussed in detail in prior studies (Getsinger et al. 2014; Gevorkyan et al. 2016, 2018). A few additional datasets were taken here with a Quantel Evergreen 30266 Nd:YAG laser with similar characteristics.

Diethyl hexyl sebacate (DEHS) oil was utilized for seeding the jet flow in PIV experiments by diverting part of the jet fluid injection line through a TSI particle generator. For the cross-flow, a commercial fog machine (Pea Soup Rocket) atomized and then injected glycol-based smoke fluid particles of 0.2 µm mass-median diameter into the cross-flow blower inlet. For simultaneous PLIF and PIV measurements, in addition to DEHS oil, acetone was seeded into the jet via two acetone seeder chambers placed upstream of the jet injection system, capable of seeding acetone tracer into the jet fluid in the gas phase at the desired mole fraction, ψ . The second chamber temperature was controlled within the range of 3-18 °C, creating an acetone vapour mole fraction range of ψ up to approximately 0.218, varied to achieve the desired fluorescence intensity for the different gas mixtures utilized in the study. Imaging for the stereo PIV system comprised two 14-bit charge-coupled device (CCD) cameras (LaVision Imager proX, 1600 × 1200 pixel resolution) separated by an approximate 60° angle with respect to the z axis. Each camera was equipped with a Nikon 60 mm lens at f/11.0, a 532.5 nm narrowband filter and a Scheimpflug lens mount; this resulted in an in-plane pixel size of approximately 120 µm for PIV studies, finer than the strain-limited diffusion scale for all flow conditions in the present study (Gevorkyan et al. 2018). The temporal interval of the two laser pulses was in the range 4–17.5 μs, depending on flow conditions, to achieve reasonable

Jet constituents	S	ψ	J_{cr}	U_j (m s ⁻¹)	μ_j (10 ⁻⁵ kg m ⁻¹ s ⁻¹)
N_2	1.0	0.0	≈ 10	7.07	1.745
N ₂ , He and acetone (PLIF/PIV)	1.0	0.112	≈ 8	6.80	1.729
N ₂ , He and acetone (PLIF)	1.0	0.218	≲7	6.49	1.653
N ₂ and He	0.35	0.0	>52	22.34	1.995
He and acetone (PLIF/PIV)	0.35	0.113	≈41	22.14	1.964

TABLE 1. For various jet gas constituents with increasing acetone mole fraction, ψ , shown are mean jet velocity and absolute viscosity required for matching $Re_j = 1900$ for two different density ratios, S = 1.0 and 0.35. Values of the estimated critical momentum flux ratio J_{cr} based on hot-wire measurements are also given.

correlation between two frames over the entire field of view. Further details on the experimental configuration and laser diagnostics may be found in Shoji (2017) and Gevorkyan *et al.* (2018).

3. Results

3.1. Shear layer instabilities for different jet mixtures

Prior experimental studies provide extensive evidence that the USL for the equidensity flush nozzle-injected JICF, consisting of pure N₂ injected into air, becomes globally unstable when J is brought to or below $J_{cr} \approx 10$ (Megerian et al. 2007; Davitian et al. 2010), or that the low-density JICF consisting of He-N2 mixtures becomes absolutely/globally unstable when $J \lesssim 10$ and/or $S \lesssim 0.40$ (Getsinger et al. 2012). Among the most compelling pieces of evidence for this transition is the significant alteration in hot-wire-based USL spectral characteristics with changes in flow conditions, although there are many additional documented features associated with this transition (Davitian et al. 2010). The hot wire is traversed along the USL trajectory coordinate s/D (see figure 1), determined based on a power-law fit to the maximum gradient in the local vertical velocity field. For the low-density JICF (S < 1) and hence for continuously varying density fields, which present difficulties in hot-wire velocity calibration, the USL trajectory as well as spectral characteristics may be determined based on uncalibrated hot-wire voltage (Getsinger et al. 2012) since the uncalibrated hot-wire signal still yields the same frequency content at various locations as a calibrated hot wire.

In the present experiments, spectral characteristics of the JICF were acquired via hot-wire anemometry for the same overall flow conditions (Re_j , J, S) but with different mixtures of species in the jet fluid. These mixtures corresponded to experiments employing different optical diagnostics. Relevant parameters are quantified in table 1 for both equidensity and low-density (S=0.35) flush nozzle-injected jets for the case $Re_j=1900$. Gas constituents included pure nitrogen associated with earlier equidensity experiments (Megerian *et al.* 2007; Getsinger *et al.* 2012) and mixtures of nitrogen and helium with acetone for simultaneous PLIF/PIV ($\psi=0.112$) and for higher-resolution PLIF-only experiments ($\psi=0.218$) typically used to quantify molecular mixing (Gevorkyan *et al.* 2016). Gas constituents corresponding to the simultaneous PLIF/PIV experiments did not include DEHS oil so as to enable hot-wire usage for spectral measurements.

Figure 3 shows fine-resolution spectral magnitude contour plots for the equidensity JICF, representing the hot-wire response to vertical velocity fluctuations measured along the USL trajectory s/D, for a fixed jet Reynolds number ($Re_i = 1900$) with different momentum flux ratios J. Data are shown for different mixtures of species in the jet fluid, corresponding to different mole fractions of acetone: $\psi = 0$ for the pure N₂ jet (approximately the same as for PIV-only experiments), $\psi = 0.0112$ for typical simultaneous PLIF/PIV experimental conditions and $\psi = 0.218$ for the typical PLIF-only experiments. Interestingly, while the overall change in USL spectral characteristics from convectively unstable (CU) behaviour at J = 41 to absolutely unstable (AU) or globally unstable (GU) behaviour at J = 5 was similar, there were subtle differences as transition from CU to AU took place, based on ψ . Interestingly, despite the careful matching of Re_i , S and J values here, the mixture of constituent gases in the jet affected the evolution of USL, both qualitatively and quantitatively. This observation will be discussed and explored further below. At J=41, 20 and 12, multiple spatially evolving instabilities in the USL were observed, with frequency shifting along the trajectory s/D resulting from tonal interference between the successively strengthening shear layer instability and the hot-wire probe (Hussain & Zaman 1978; Getsinger et al. 2012). The average of the shifting frequencies was considered to correspond to a fundamental frequency f_o , as done in prior studies (Megerian et al. 2007; Davitian et al. 2010; Getsinger et al. 2012). Subharmonic development, representing vortex merger, was more prominent at these higher J values, while higher harmonics appeared to be strengthened with a reduction in J as cross-flow velocity U_{∞} increased. These spectral characteristics corresponded to the behaviour of a convectively unstable USL, as discussed in prior JICF stability studies (Megerian et al. 2007; Davitian et al. 2010; Getsinger et al. 2012). But with the addition of increasing concentrations of acetone, and with the presence of helium and nitrogen designed to create S = 1, the location of initiation of the instability (s/D)was delayed, especially as J was reduced, suggesting a slight weakening of the shear layer instability with increasing acetone concentration. There were also increases in the estimated average fundamental frequency f_o and hence Strouhal number St_o associated with the initiation of the instability as ψ was increased.

As the momentum flux ratio was reduced to the range close to initiation of an absolutely unstable USL for the pure nitrogen jet, near J=10 (Megerian et al. 2007; Davitian et al. 2010; Getsinger et al. 2012), figure 3(d) indicates that the effect of acetone in the jet mixture was not only to delay the onset of the instability, but to cause its characteristics to be associated with convective instability rather than the pure-tone, spatially invariant absolute instability observed for $\psi=0$ at this flow condition. Even at J=8 (figure 3e), there was evidence of a weakening of the shear layer, with a very low level of tonal interference, especially at $\psi=0.218$, which typically would not be classified as characteristic of GU flow. At a much lower value of J=5, shown in figure 3(f), all jet mixtures produced the typical AU/GU behaviour, with a strong pure-tone instability initiated close to the jet exit, a clear fundamental frequency f_0 and the absence of subharmonic disturbances. For these lower J values there were nevertheless small increases in St_0 with increasing ψ .

To verify that the phenomena observed in figure 3 reflected actual USL behaviour and that acetone itself was not affecting hot-wire performance, spectral measurements were also made outside of the USL, where there was little or no acetone present. For these spectral measurements the hot-wire probe was initially situated at a fixed USL trajectory location then traversed upstream, in the negative x direction, fixing y and z locations. There were no substantive alterations in spectral character (other than



T. Shoji and others

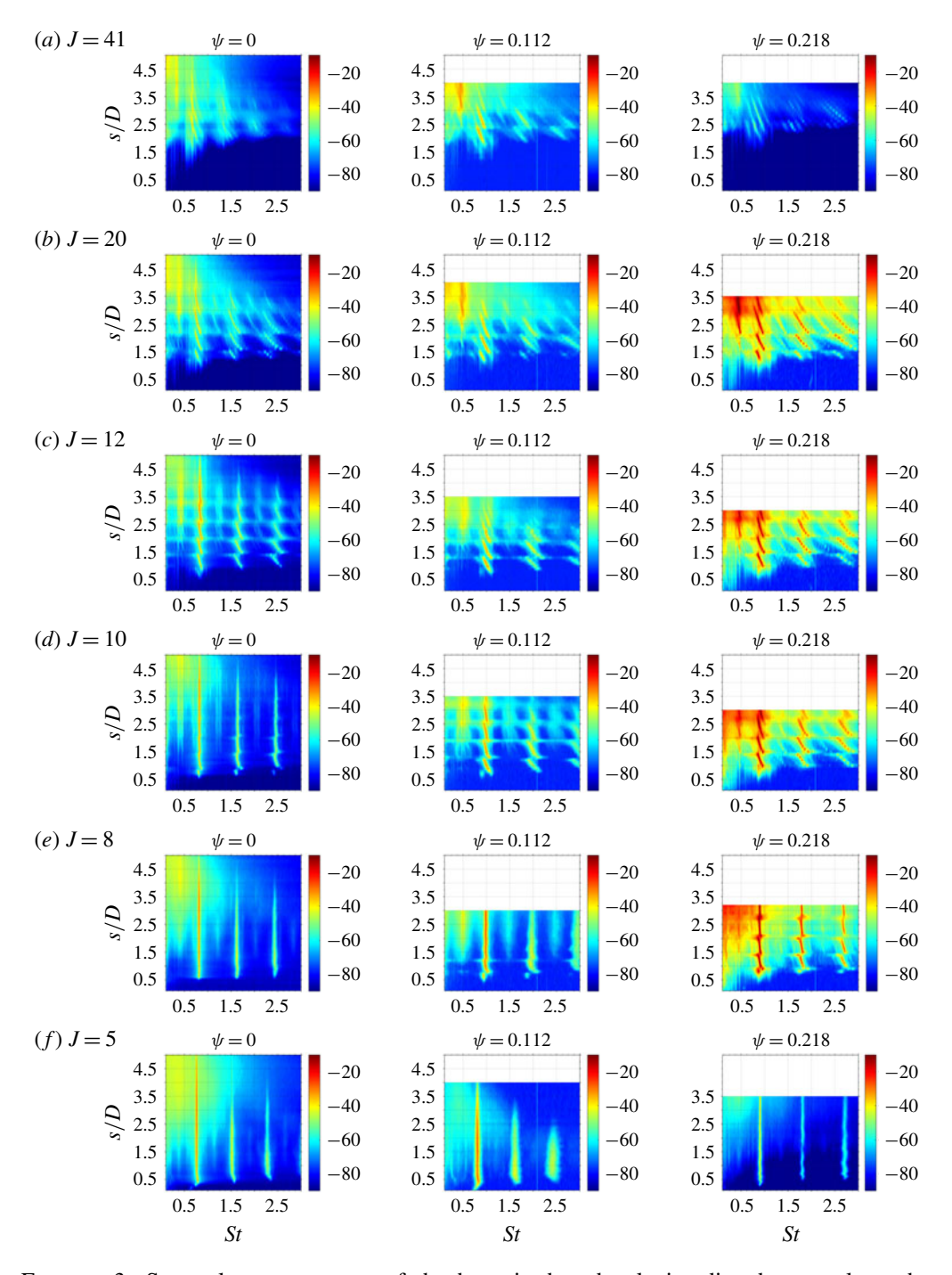


FIGURE 3. Spectral contour maps of the hot-wire-based velocity disturbances along the USL trajectory coordinate s/D for the JICF at $Re_j = 1900$ and S = 1.0 with varying J and acetone mole fraction ψ , corresponding to jets with N_2 only ($\psi = 0$, reproduced from original data in Getsinger *et al.* (2012)), the jet mixture for simultaneous PLIF and PIV ($\psi = 0.112$) and the PLIF-only experiments ($\psi = 0.218$). The colour bar represents disturbance amplitude in dB.

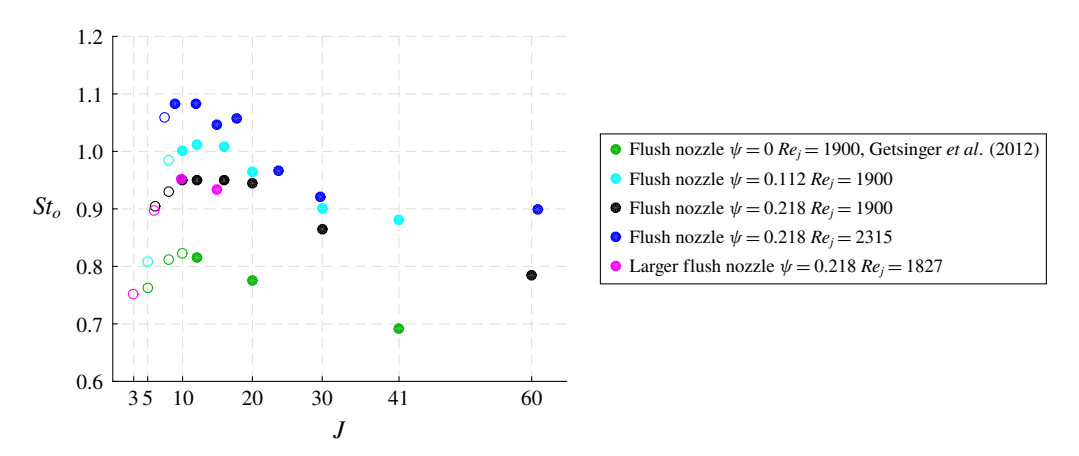


FIGURE 4. Variation in Strouhal number St_o for the fundamental USL mode based on jet diameter and mean jet velocity U_j as a function of J for the equidensity flush nozzle-and larger flush nozzle-injected JICF. Data are shown for Re_j and acetone mole fractions ψ . Filled and open symbols represent the hot-wire-determined convectively and globally unstable USL, respectively.

strength of the instabilities) as the hot wire was moved outside of the USL into the air cross-flow and, in addition, St_o did not vary. Thus it was determined that alterations in the USL transition and J_{cr} for the acetone-seeded JICF reflected actual physical phenomena and were not affected by the measurement method.

Similar alterations in fundamental St_o values and J_{cr} were observed in other acetone-seeded JICF experiments for a range of operating conditions, where deviations from established values of J_{cr} occurred when acetone was present in the jet fluid. Yet overall trends associated with the variation in St_o with J were consistent with prior equidensity flush nozzle-injected JICF results in the absence of acetone (Megerian et al. 2007). This is shown in figure 4 for various equidensity flow conditions, with different Re_i values, gas constituents and two different nozzle diameters. For a fixed Re_i and acetone concentration, as J was reduced from a large value by increasing the cross-flow velocity, frequency f_o and hence St_o values from hot-wire-based spectra corresponding to convectively unstable flow always increased before reaching a peak at $J \approx J_{cr}$, and then decreased after the transition to global instability for $J < J_{cr}$. Figure 4 demonstrates a minimal influence of jet diameter for the same Reynolds number (e.g. comparing black and purple symbols), but a somewhat larger influence of Re_i and ψ on J_{cr} (e.g. comparing green and dark blue symbols). Increasing the mole fraction of acetone appeared to reduce the value of J_{cr} , seen as the J value at which the closed or filled symbols became open ones for a given set of conditions in figure 4. For a given S and Re_i , a smaller J_{cr} corresponded to an increase in the cross-flow velocity U_{∞} required to create transition to absolute instability. Increasing acetone concentrations also caused an increase in f_o and hence in St_o , consistent with spectral contour plots (figure 3).

The reduction in hot-wire-estimated J_{cr} with increasing concentrations of acetone in the jet fluid is recorded in table 1 for both equidensity and low-density flush nozzle-injected jets for experiments with a fixed $Re_j = 1900$. Because jet density and Reynolds number were matched in these experiments for each J value studied, and because the absolute viscosity of the mixture did vary among the cases for different

concentrations of acetone, as determined via the Wilke formula (Bird *et al.* 1960) and the Reichenberg method (Poling *et al.* 2001), the actual mean jet velocity U_j at the exit plane necessarily differed slightly for the different acetone concentrations with otherwise constant bulk flow properties. The changes in J_{cr} observed in figure 4 and in table 1 with acetone addition may be interpreted in the context of flow in the vicinity of the USL near the injection location, as will be shown.

3.2. Analogy to counter-current shear layer

Iyer & Mahesh (2016) computationally demonstrate the phenomenological similarity in the USL instability transition for the flush nozzle-injected transverse jet to that for the CCSL based on the CCSL velocity ratio R_1 in the centre plane, defined in (1.1). The present study explored this similarity based on numerous experimental datasets, using velocities extracted from PIV-only data for density ratios S = 1.00, 0.70, 0.55 and 0.35 (without the presence of acetone in the jet), taken from Getsinger (2012), and also using the PIV portion of simultaneous PLIF and PIV experiments at S = 1.00 and 0.35, many of which were taken from Shoji (2017) and Gevorkyan *et al.* (2018). Hence the acetone mole fractions in this comparison were relatively small, $\psi = 0.112$.

To extract the mixing layer (CCSL) velocity ratio R_1 from PIV-based data, the same method as that used computationally in Iyer & Mahesh (2016) was applied. First, the USL was defined by the magnitude of mean vorticity in the out-of-plane direction, $|\omega_v|$, as shown, for example, in figure 5(a) for the equidensity JICF with J=20. The normal direction to the USL, n/D, may be defined from the $|\omega_v|$ field, displayed using multiple lines close to the jet exit in figure 5(a). As done in the numerical studies (Iyer & Mahesh 2016), mean vertical velocity distributions then can be extracted at different locations s/D just downstream of the jet exit, along the layer-normal direction n/D, as shown in figure 5(b). These velocity distributions were observed to have regions of both negative vertical velocity upstream of the USL centre and positive vertical velocity within the jet but outside of the USL, including a fairly uniform velocity profile near the jet centre, consistent with a nozzle-generated top-hat-like exit profile (examples of which, for a range of conditions, may be found in Gevorkyan et al. (2018)). The near-field velocity profiles in figure 5(b) appeared quite analogous to those for a CCSL, and hence V_1 and V_2 could be extracted from such PIV-based data to evaluate the CCSL velocity ratio R_1 via (1.1). More details on the method of estimation of R_1 for the JICF may be found in Iyer & Mahesh (2016). In the present experiments, the region upstream of the layer for which negative (vertically downward) flow occurred extended to distances in the negative layer-normal direction that depended on J. This negative flow region extended to approximately $n/D \approx -0.5$ for higher J values such as J = 41, but for lower J values such as J = 5, this region extended further, to $n/D \approx -2.0$.

Resultant R_1 values for a range of experimental conditions with the flush nozzle are shown in figure 6(a) for the equidensity JICF and in figure 6(b-d) for the low-density JICF at density ratios S equal to 0.70, 0.55 and 0.35, respectively. Filled and open symbols represent convectively and absolutely/globally unstable transverse jet USL conditions, respectively, determined experimentally via hot-wire-measured spectral characteristics such as those shown in figure 3. In addition, for most of the cases in figure 6(a-d), separate PIV-based proper orthogonal decomposition (POD) mode coefficient plots were examined to verify consistency with AU shear layer identification. As described in detail in Meyer, Pedersen & Özcan (2007) and Gevorkyan *et al.* (2018), using snapshot POD analysis of the PIV-based jet centre

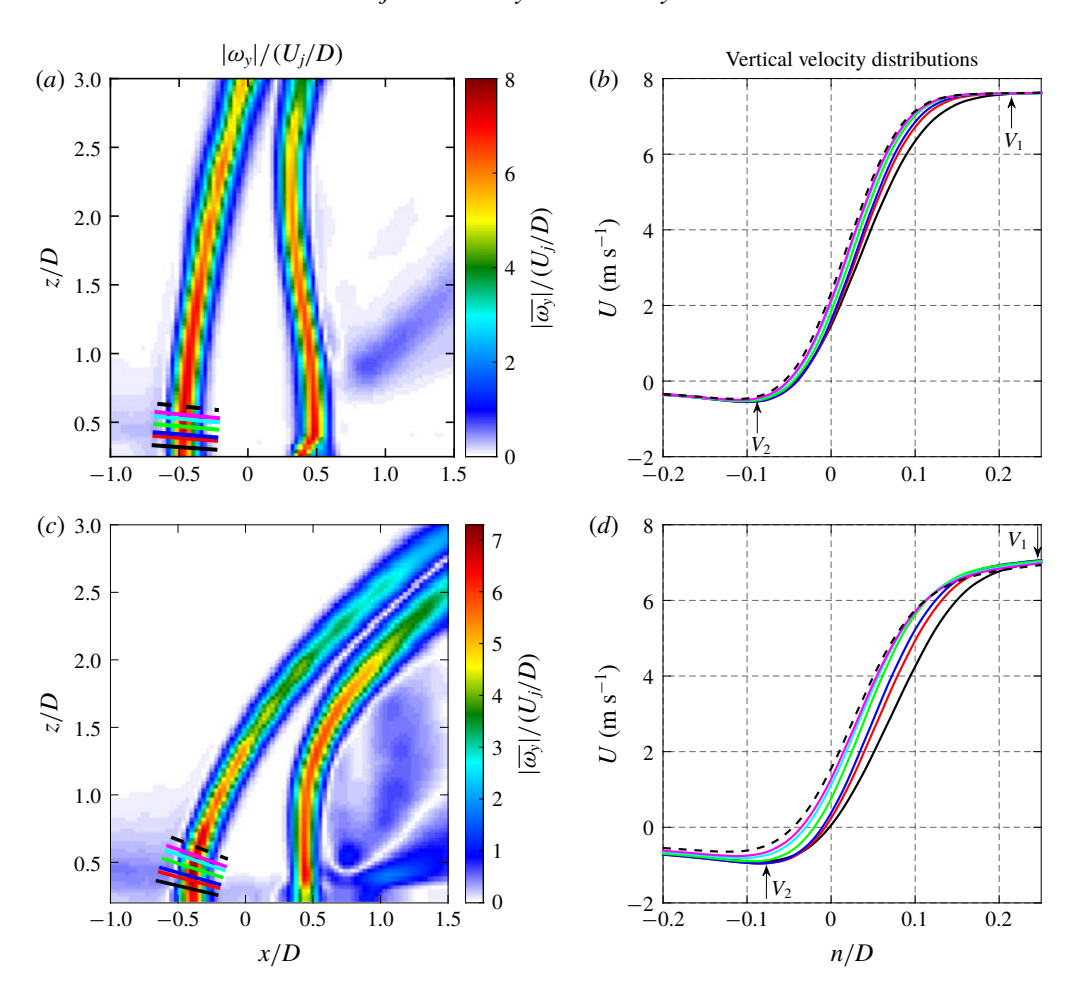


FIGURE 5. (a,c) Normalized magnitude of vorticity in the out-of-plane direction, $|\omega_y|$, for J=20 and J=5, respectively. (b,d) Vertical mean jet velocity distributions in the USL trajectory-normal direction, n/D, at variable trajectory locations, s/D, corresponding to J=20 and J=5, respectively, with the same line colours as in parts (a,c). Flow conditions correspond to the equidensity, nozzle-injected JICF with $Re_i=1900$ and $\psi=0.112$.

plane data, plots of the POD coefficients of the first and second modes become circular when there is a periodic travelling wave flow structure consistent with an absolutely unstable USL. Such behaviour in the PIV-based experiments was used to verify consistency with the stability condition for the USL identified via hot-wire anemometry and indicated by the open circles in figure 6. The dashed lines in each panel indicate the established (theoretical) 2-D CCSL velocity ratio, $R_{1,cr(th)}$, for transition from a CU to AU shear layer for the given density ratio. These values are predicted by inviscid linear stability theory for the planar CCSL with S=1 from Huerre & Monkewitz (1985). For S<1, theoretical values of $R_{1,cr(th)}$ were extracted from the study by Pavithran & Redekopp (1989) for the CCSL, although it is noted that use of the Crocco–Busemann relation to compute density profiles can be inaccurate in representing the near field and thus in prediction of stability characteristics for light and hot jets (Coenen & Sevilla 2012). For all cases in figure 6,



T. Shoji and others

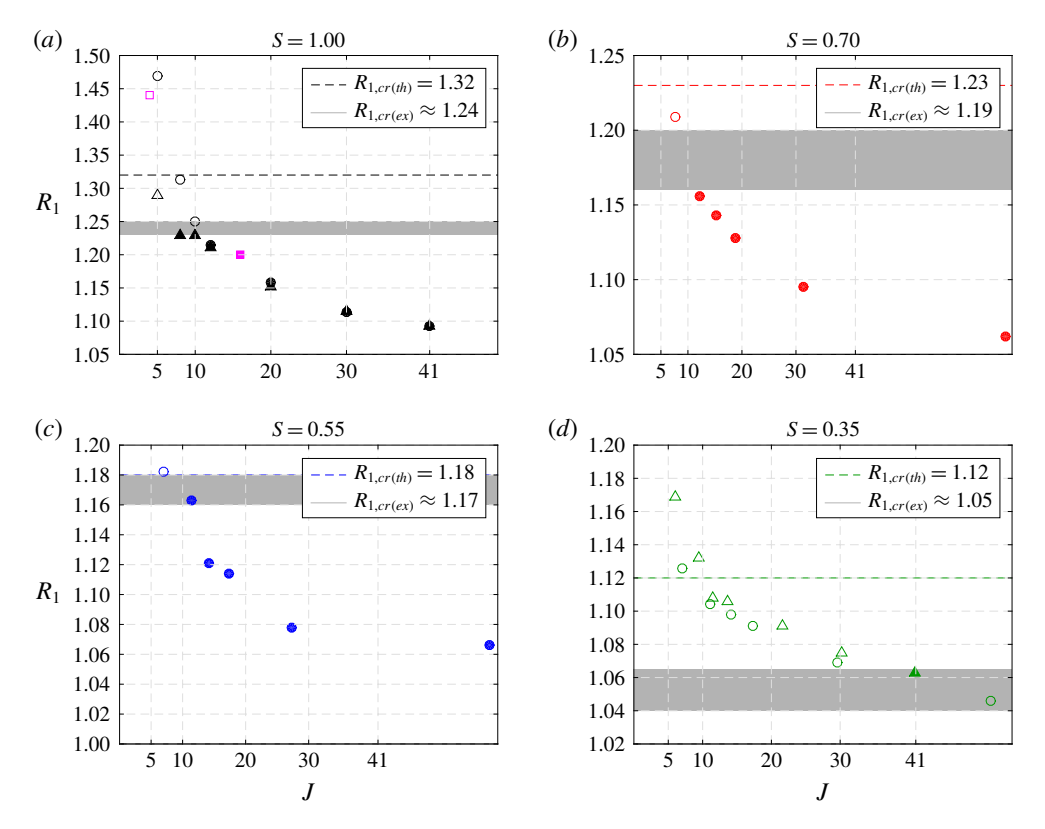


FIGURE 6. Data points show R_1 versus J for the JICF at different density ratios S for a fixed $Re_j = 1900$. Dashed lines corresponding to the colour of data points represent the theoretical velocity ratio, $R_{1,cr(th)}$, for the 2-D CCSL, while the grey region represents the range of experimentally observed values, $R_{1,cr(ex)}$. Circles represent R_1 values extracted from PIV-only experiments, while triangle symbols are based on data from simultaneous PLIF/PIV experiments with acetone at $\psi \approx 0.112$. Filled and open symbols represent convectively and absolutely/globally unstable conditions, respectively, determined via hot-wire anemometry. In (a), the purple squares represent R_1 determined from equidensity DNS by Iyer & Mahesh (2016) at $Re_i = 2000$.

dashed lines theoretically distinguish convectively unstable conditions ($R_1 < R_{1,cr}$) from absolutely unstable conditions ($R_1 > R_{1,cr}$) for the CCSL. The transition from filled to open symbols in the panels enables estimation of the experimentally determined value or range of values for the critical velocity ratio, $R_{1,cr(ex)}$, indicated by the shaded regions in figure 6.

For the equidensity JICF without acetone in figure 6(a) (circles), corresponding to PIV-only experiments from which V_1 and V_2 were extracted, AU conditions occurred when $J \lesssim 10$ according to hot-wire measurements. The corresponding value of R_1 at this AU transition was approximately 1.24, below the theoretical critical value, $R_{1,cr(th)} = 1.32$. While there was a quantitative difference in the critical value of R_1 , as one might expect for comparisons of a round, deflected shear layer with an idealized planar shear layer separated by infinite flow regions, the trends in figure 6(a) were consistent with the concept of the CCSL. That is, lower J values producing absolute instability in the transverse jet corresponded to larger

 R_1 values, exceeding a critical value and thus being consistent with a self-excited CCSL. Hot-wire-determined convectively unstable conditions, with filled symbols in figure 6(a), similarly corresponded to $R_1 < R_{1,cr(ex)} \approx 1.24$. These trends were also consistent with the DNS results for two different velocity ratios computed by Iyer & Mahesh (2016), shown for reference in figure 6(a). These two computed data points for R_1 not only straddled the experimentally estimated value $R_{1,cr(ex)} \approx 1.24$, but also were consistent with the trends in the range of values shown by the experimental data points (circles, in the absence of acetone).

For the equidensity experiments with acetone present, V_1 and V_2 extracted from the PIV portion of simultaneous PLIF and PIV measurements showed small yet systematic reductions in V_1 and less-negative values of V_2 as compared with extracted values in PIV-only experiments at the same J and Re_i . These changes are reflected in the altered values of R_1 shown by the triangle symbols in figure 6(a), where the critical condition changed to $J_{cr} \lesssim 8$, with $R_{1,cr(ex)} \approx 1.23$. The differing J_{cr} values associated with USL transition with and without acetone in figure 6(a) appeared to be associated with the slightly altered USL CCSL-like velocity distributions and the resulting small differences in the values of V_1 and V_2 close to the jet's exit, thus producing a slightly different R_1 . These differences in the velocity distributions resulted from small differences in the mean exit velocity U_i that were required to match both Re_i and S for a given J when the jet mixture contained acetone, with a different overall absolute viscosity μ_i , as noted in § 3.1. Hence, while in both equidensity cases in figure 6(a) there was consistency in trends in the USL instability transition (from CU to AU, corresponding to increases in R_1), there was a small quantitative difference in $R_{1,cr}$ as well as in J_{cr} .

For the low-density JICF, trends in increasing R_1 with a reduction in J at matched Re_i and S were also consistent with the CCSL model, shown in figures 6(b), 6(c), and 6(d). The theoretical value of $R_{1,cr(th)}$ determined from Pavithran & Redekopp (1989) was somewhat larger than the PIV-based value of $R_{1,cr(ex)}$ for density ratio S = 0.70 (figure 6b), though the band in which the transition from CU to AU took place (at $J_{cr} \lesssim 10$) was relatively wide in terms of estimating the critical R_1 range. For S = 0.55 (figure 6c), the theoretical value of $R_{1,cr(th)}$ was slightly higher than the band at which PIV-only experiments indicated a transition from convective to absolute instability. Consistent with findings in Getsinger et al. (2012), the very-lowdensity conditions for S = 0.35 in figure 6(d) generally showed absolutely unstable USL conditions for virtually all J values explored. An exception for the case with acetone present occurred at J=41, where the spectra were not quite the same as those associated with absolute instability, with a small degree of tonal interference. This condition for J = 41 and S = 0.35, which may have been marginally convectively unstable, produced CCSL velocity profiles corresponding to $R_1 \approx 1.065$, well below that of the theoretical critical value of $R_{1,cr(th)} = 1.12$ for this density ratio. We note that in Getsinger et al. (2012) hot-wire measurements indicated that either J < 10or S < 0.40 produced an absolutely/globally unstable USL, but data in figure 6(d)suggested that a J value greater than 41 at S = 0.35 in the presence of acetone, or potentially greater than J = 52 without acetone, could produce a convectively unstable USL, although such conditions were not attainable in the present experiments. Overall, then, there was general consistency between JICF shear layer transition and transition in a CCSL model from convective to absolute instability, even though the critical values of R_1 were typically smaller in the experiments than from the inviscid 2-D CCSL analysis. These findings suggest that the mechanism by which the JICF USL transition takes place, at least for the flush nozzle, could relate to the strengthening local counter-flow occurring at the jet exit.

It should be noted that the CCSL model here also provided some evidence for a mechanism for the development of the self-sustained global instability in the jet's USL. Huerre & Monkewitz (1990) note that, as a flow transitions from convective to absolute instability, a 'zone of local absolute instability' forms. As the zone grows beyond a critical size, the system can become globally unstable, with a Hopf bifurcation to a self-sustained global mode. Huerre and Monkewitz note that the existence of this region of local absolute instability is a necessary though not sufficient condition for the existence of an amplified global mode. Evidence of global instability in the flush nozzle-injected transverse jet for a small enough J value, including evidence of a Hopf bifurcation (Davitian et al. 2010; Regan & Mahesh 2017), has already been documented both experimentally and computationally. The region of negative flow upstream of injection for the transverse jet, found here to grow in the negative n/D direction as cross-flow velocity was increased (e.g. as in figure 5), could indeed represent this growing 'zone of absolute instability', providing additional evidence for transition to a global mode. This phenomenon appeared to occur even for the somewhat thick CCSLs created by this nozzle, as will be discussed

Additional features of the CCSL for which experimental data from the round JICF may be compared with 2-D theory include the Strouhal number associated with the fundamental shear layer instability but where the length scale of interest is the momentum thickness of the local near-field CCSL shown in figure 5. The linear stability theory of Huerre & Monkewitz (1985) for the equidensity 2-D CCSL suggests that the critical velocity ratio $R_{1,cr} = 1.315$ corresponds to a non-dimensional frequency of 0.192, which may be written in terms of a momentum-thickness-based Strouhal number $St_{\theta} \equiv f_{o}\theta_{o}/2\bar{V} = 0.0153$, where the average velocity in the CCSL takes the form $\bar{V} \equiv \frac{1}{2}(V_{1} + V_{2})$. For the 2-D CCSL in figure 5(b), the momentum thickness in the near-field region of the layer may be approximated as

$$\theta_{CCSL} = \int_{n_{V_2}}^{n_{V_1}} \frac{u(n) - V_2}{V_1 - V_2} \left(1 - \frac{u(n) - V_2}{V_1 - V_2} \right) dn, \tag{3.1}$$

where the limits of integration represent locations in the layer-normal direction at which the velocities reach the values of V_1 and V_2 . Strykowski & Niccum (1991) compare an experimentally determined Strouhal number with the theoretical value of Huerre & Monkewitz (1985), but alter the limits of integration for (3.1) so that the lower limit is chosen to minimize uncertainties caused by very low velocities in the vicinity of the negative counter-flow. That lower limit n_L corresponds to the location at which $(u - \bar{V})/(V_1 - V_2) = -0.4$. This produces a momentum thickness designated here as θ_{n_I} . On this basis, the Strouhal number extracted from the Strykowski & Niccum (1991) experiments at $R_1 = 1.4$ (above the critical limit) is $St_{\theta_{n_l}} = 0.0185$. At a velocity ratio below the critical limit for the transition to absolute instability for the CCSL, at $R_1 = 1$, Strykowski & Niccum (1991) observe that $St_{\theta_{n_l}} = 0.012$, in agreement with the Strouhal number associated with the free jet shear layer by Hussain & Zaman (1978). Hussain & Zaman (1978) note the prevalence of a 'shear layer mode' at which vortex pairing has occurred, hence is associated with the subharmonic mode for the free jet, downstream of the spatial locations at which the authors observe tonal interference by a hot-wire probe producing frequency shifting of the fundamental mode; such subharmonic modes were seen for the transverse jet at higher momentum flux ratios, e.g. in figures 3(a-c).

In the present experiments for the JICF, one can make quantitative comparisons with the theoretical 2-D CCSL-based Strouhal numbers by evaluating relevant CCSL

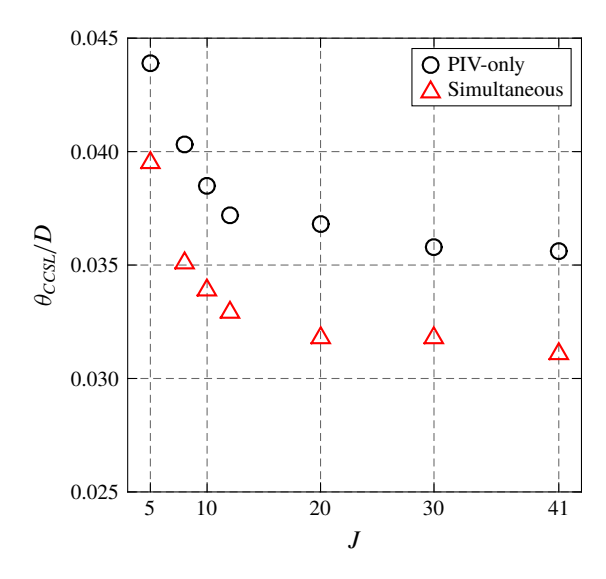


FIGURE 7. Variation in momentum thickness θ_{CCSL} (scaled by D) for the local CCSL as a function of J for the equidensity JICF at $Re_j = 1900$. Results for data extracted from PIV-only experiments, without acetone, and simultaneous PLIF/PIV experiments, with acetone present at $\psi \approx 0.112$, are shown.

momentum thicknesses, either based on the definition in (3.1) for θ_{CCSL} or based on θ_{n_L} . Figure 7 shows the variations in momentum thickness θ_{CCSL} with J for the equidensity JICF at $Re_j = 1900$. The aforementioned differences in velocity magnitudes V_1 and V_2 with and without acetone, resulting from the effects of acetone on absolute viscosity and thus on the mean jet velocity U_j and cross-flow velocity U_∞ required to match Re_j and S for a given J, affected the CCSL velocity profiles and hence the momentum thicknesses. With the addition of acetone at the mole fraction shown for simultaneous PLIF and PIV, $\psi \approx 0.112$, figure 7 showed a reduction in non-dimensional momentum thickness θ_{CCSL}/D of approximately 17% for the range of J values shown. Corresponding values of θ_{nL}/D showed a similar reduction.

These differences in non-dimensional momentum thickness with and without acetone provided additional insights into the possible reasons for observed differences in the values of the critical CCSL velocity ratio R_1 for the equidensity cases with and without acetone shown in figure 6(a). One would expect that the quantitative nature of the instabilities should be the same, based on the flow field's dependence on non-dimensional parameters J, Re and S for a given transverse jet condition. The differences in the USL and the instabilities with and without acetone for the same values of these non-dimensional parameters suggested that an additional non-dimensional parameter could be relevant to the nature of the instabilities, per non-dimensional analysis. This non-dimensional parameter appeared to be the ratio of the jet-to-cross-flow absolute viscosities, μ_j/μ_∞ , causing the scaled CCSL momentum thickness θ/D to be dependent on the presence of acetone, as shown in figure 7. This issue will be discussed further below.

It is noted that the relatively large momentum thicknesses in figure 7, for example, producing D/θ_{CCSL} values as large as 32 for J=41 with acetone and as small as 23 for J=5 without acetone, were thicker than those typically considered to be thin enough so that shear layer curvature effects may be considered negligible (D/θ) of

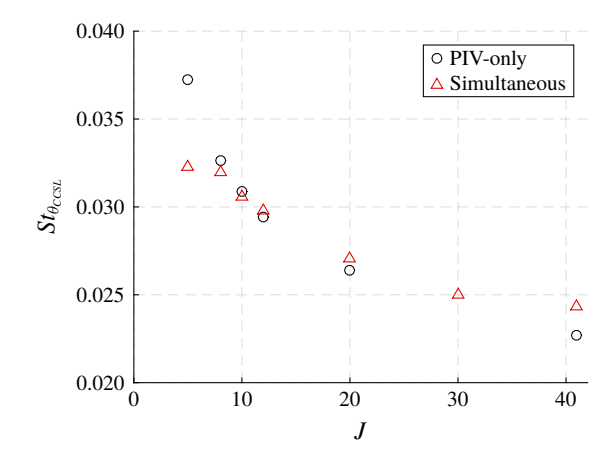


FIGURE 8. Variation in Strouhal number based on momentum thickness, $St_{\theta_{CCSL}} \equiv f_o\theta_{CCSL}/2\bar{V}$, as a function of J for the equidensity JICF case at $Re_j = 1900$. Results for data extracted from PIV-only experiments, without acetone, and simultaneous PLIF/PIV experiments, with acetone present at $\psi \approx 0.112$, are shown.

the order of 50, per Huerre & Monkewitz (1985), and larger, of the order of 230, by Strykowski & Niccum (1991)). The momentum thickness can impact application of planar CCSL inviscid instability theory in predicting fundamental instability frequencies, as noted by Strykowski & Niccum (1991). For example, LSA for the planar CCSL (Jendoubi & Strykowski 1994) suggests that the critical value of $R_{1,cr}$ can change with more significant reductions in D/θ , which in the case of the JICF would correspond to lower J conditions, e.g. J = 5. Yet the actual experimental values of R_1 for this range of momentum thicknesses and J values shown in figure 6(a) were very close to DNS-based results (Iyer & Mahesh 2016) for similar flow conditions. For the strongly deflected jet in cross-flow, one would expect curvature effects in the round jet as well as the increasingly non-parallel flow along the curved USL to be inconsistent with an idealized 2-D CCSL, as also noted by Iyer & Mahesh (2016). Nevertheless, it is remarkable that the quantitative prediction of transition to JICF global instability was generally close to values of $R_{1,cr(th)}$ predicted by inviscid 2-D LSA, both with and without the presence of acetone, indicated in figure 6. Hence it was of interest to utilize momentum thickness in comparing the present instability frequencies with established ranges of Strouhal number for the planar CCSL.

Figure 8 shows the variation in Strouhal number based on θ_{CCSL} derived from PIV-only and simultaneous PLIF/PIV experimental datasets for the equidensity JICF at $Re_j = 1900$. Remarkably, for a Strouhal number based on CCSL-based momentum thickness scaling rather than diameter D, and based on twice the average velocity in the CCSL, $2\bar{V}$ rather than average jet velocity U_j (which does not capture the effect of the local negative flow upstream of the jet), there was a generally good collapse of the data for cases with and without acetone in the jet fluid. An exception was seen in the case of the very low momentum flux ratio jet, with J = 5, which as noted previously had the thickest and most deflected USL. It is remarkable that St_θ values with and without acetone at a given J value collapsed onto one another for most cases in figure 8, in contrast to the differing Strouhal numbers based on diameter and mean jet velocity in figure 4, shown by data points indicated in green and cyan. The results in figure 8 thus provided further evidence for the importance of

the non-dimensional parameter θ/D , related to differences in jet fluid viscosity, and the relevance of the CCSL model in interpreting JICF shear layer instability transition. For the clearly convectively unstable flows at J = 41, for example, St_{θ} was of the order of 0.023–0.024, corresponding to St_o values of approximately 0.7 without acetone and approximately 0.9 with an acetone mole fraction $\psi = 0.112$ (figure 4). These frequencies corresponded to the fundamental mode for the convectively unstable JICF with spectral characteristics as in figure 3(a); the observed subharmonics thus had St_{θ} values of the order of 0.011–0.012. The J = 41 condition here produced $R_1 \approx 1.09$, below the experimentally observed critical condition for the CCSL, $R_{1,cr} \approx 1.24$. These measured Strouhal numbers associated with $R_1 \approx 1.09$ were approximately twice as large as those observed for the free jet by Hussain & Zaman (1978) and Strykowski & Niccum (1991) at $R_1 = 1.0$. As J was reduced and the critical condition for transition to global instability approached in figure 8, the values of St_{θ} increased to the range of 0.03 (J = 10) to 0.037 (J = 5) with acetone), also approximately twice as large as established theory and experiments for the planar CCSL (Huerre & Monkewitz 1985; Strykowski & Niccum 1991). The well-established trend for the CCSL, whereby Strouhal number increases rather abruptly as one approaches the critical condition (Strykowski & Niccum 1991), is consistent with observations in figure 8.

These differences in fundamental Strouhal number St_{θ} between the present experiments and the established 2-D CCSL values were probably not so much the result of slightly different CCSL velocity ratios R_1 at transition as the relatively large CCSL momentum thickness at and beyond critical conditions, as noted previously. More importantly, Huerre & Monkewitz (1990) note that the frequency selection criterion for global instability depends on how the absolutely unstable frequency evolves spatially, which in turn depends on the development of the base flow for the flow field. The spatial development in a counter-current, planar mixing layer is typically much slower than the spatial development observed in a transverse jet, as indicated in earlier transverse jet stability studies (Alves *et al.* 2007, 2008), and the global frequency determination here is not a local feature of the flow, in contrast to the determination of the critical parameter ($R_{1,cr}$) for the onset of absolute instability. Hence in many respects one would not expect the JICF Strouhal numbers St_{θ} to correspond very closely to the established values for the planar CCSL.

4. Discussion and conclusions

This experimental study provides evidence that the phenomena associated with the USL instability transition for the flush nozzle-injected transverse jet can be understood in the context of transition in the CCSL instability. Consistent qualitative and quantitative trends in flow conditions creating convective versus absolute/global instability in the USL, and comparisons with established trends from planar LSA predictions (figure 6), speak to the importance of the degree of counter-flow just upstream of the jet exit. Further insights may be gleaned from noting that the region of negative flow forming upstream of injection for the transverse jet, measured here to grow in the negative n/D direction as cross-flow velocity was increased, could indeed represent a growing 'zone of absolute instability', based on J, a necessary requirement for transition of the instability to a global mode (Huerre & Monkewitz 1990).

Alterations in the Strouhal number associated with the USL instabilities with a reduction in momentum flux ratio J, while approaching the critical CCSL velocity ratio, $R_{1,cr}$, were also consistent with established trends observed for the CCSL,

with a collapse of frequency data when Strouhal number was scaled in terms of momentum thickness. The St_{θ} values in the present study for a range of J values were approximately twice as large as theoretical values for the equidensity 2-D CCSL (Huerre & Monkewitz 1985; Strykowski & Niccum 1991). It is likely that an altered theoretical exploration of the CCSL, an LSA applied to a round jet shear layer with external counter-flow, could provide improved comparisons with the present experiments.

Interestingly, in the DNS for the flush nozzle-generated JICF by Iyer & Mahesh (2016), the convectively unstable USL condition (J=16) produces spectral characteristics in which a lower frequency, corresponding to $St_o=0.39$ (based on diameter), is initially observed to occur close to the jet exit, at a location s/D=0.1. This value is half that of the fundamental instability observed in experiments (Megerian *et al.* 2007). But then a bit further along the shear layer, for $s/D \ge 1.0$, the same Strouhal number as in experiments is found to dominate the flow ($St_o=0.78$, as shown in figure 4). This observation could be attributed, as suggested by Iyer & Mahesh (2016), to the very low amplitude of the initial spectral peak observed in the computations, below the noise floor for hot-wire measurements in the experiments. The dominance of the $St_o=0.78$ fundamental mode for that flow condition in the DNS, and consistency with experiments for that condition and for Strouhal numbers associated with global instability at J=4, suggests that the frequencies quantified in the present study could well be physically relevant to those predicted via DNS.

Ultimately, the general consistency between the degree of counter-flow required for CCSL transition and transition in the transverse jet's USL enables new insights into the dynamical mechanisms associated with the JICF. Clearly, a more robust comparison of transverse jet USL instability transition with the concept of the CCSL requires that the theory represents more closely the actual round jet injected flush into a strengthening cross-flow (or at least counter-flow). Overall, however, even this simple comparison with the 2-D CCSL model provides information that can be used to control jet behaviour, for example, involving active alteration of the flow just upstream of injection to alter USL stability characteristics. This approach is the subject of ongoing studies involving control of this important flow field.

Acknowledgements

The authors wish to express their thanks to Professor L. Alves of the Universidade Federal Fluminense (UFF) for helpful discussions and insights in this study. This research has been supported by the National Science Foundation under grant CBET-1437014 and by the Air Force Office of Scientific Research under grant FA9550-15-1-0261.

Declaration of interests

The authors report no conflict of interest.

REFERENCES

ALVES, L. S. DE B., KELLY, R. E. & KARAGOZIAN, A. R. 2007 Local stability analysis of an inviscid transverse jet. *J. Fluid Mech.* **581**, 401–418.

ALVES, L. S. DE B., KELLY, R. E. & KARAGOZIAN, A. R. 2008 Transverse-jet shear-layer instabilities. Part 2. Linear analysis for large jet-to-crossflow velocity ratio. *J. Fluid Mech.* **602**, 383–401.

- BAGHERI, S., SCHLATTER, P., SCHMID, P. J. & HENNINGSON, D. S. 2009 Global stability of a jet in crossflow. *J. Fluid Mech.* **624.** 33–44.
- BIRD, R. B., STEWART, W. E. & LIGHTFOOT, E. N. 1960 Transport Phenomena. John Wiley & Sons.
- CANZONIERI, K. 2009 Experimental studies on low density jets in crossflow. Master's thesis, University of California, Los Angeles, Department of Mechanical and Aerospace Engineering.
- COENEN, W. & SEVILLA, A. 2012 The structure of the absolutely unstable regions in the near field of low-density jets. *J. Fluid Mech.* 713, 123–149.
- DAVITIAN, J., GETSINGER, D., HENDRICKSON, C. & KARAGOZIAN, A. R. 2010 Transition to global instability in transverse-jet shear layers. *J. Fluid Mech.* **661**, 294–315.
- FRIC, T. F. & ROSHKO, A. 1994 Vortical structure in the wake of a transverse jet. *J. Fluid Mech.* **279.** 1–47.
- GETSINGER, D. R. 2012 Shear layer instabilities and mixing in variable density transverse jet flows. PhD thesis, University of California, Los Angeles.
- GETSINGER, D. R., GEVORKYAN, L., SMITH, O. I. & KARAGOZIAN, A. R. 2014 Structural and stability characteristics of jets in crossflow. *J. Fluid Mech.* 760, 342–367.
- GETSINGER, D. R., HENDRICKSON, C. & KARAGOZIAN, A. R. 2012 Shear layer instabilities in low-density transverse jets. *Exp. Fluids* **53**, 783–801.
- GEVORKYAN, L., SHOJI, T., GETSINGER, D. R., SMITH, O. I. & KARAGOZIAN, A. R. 2016 Transverse jet mixing characteristics. *J. Fluid Mech.* **790**, 237–274.
- GEVORKYAN, L., SHOJI, T., PENG, W. Y. & KARAGOZIAN, A. R. 2018 Influence of the velocity field on scalar transport in gaseous transverse jets. *J. Fluid Mech.* 834, 173–219.
- HALLBERG, M. P. & STRYKOWSKI, P. J. 2006 On the universality of global modes in low-density axisymmetric jets. *J. Fluid Mech.* **569**, 493–507.
- HUERRE, P. & MONKEWITZ, P. A. 1985 Absolute and convective instabilities in free shear layer. J. Fluid Mech. 159, 151–168.
- HUERRE, P. & MONKEWITZ, P. A. 1990 Local and global instabilities in spatially developing flows. *Annu. Rev. Fluid Mech.* **22**, 473–537.
- HUSSAIN, A. K. M. F. & ZAMAN, K. B. M. Q. 1978 The free shear layer tone phenomenon and probe interference. *J. Fluid Mech.* **87**, 349–383.
- IYER, P. S. & MAHESH, K. 2016 A numerical study of shear layer characteristics of low-speed transverse jets. *J. Fluid Mech.* **790**, 275–307.
- JENDOUBI, S. & STRYKOWSKI, P. J. 1994 Absolute and convective instability of axisymmetric jets with external flow. *Phys. Fluids* **6**, 3000–3009.
- KARAGOZIAN, A. R. 2010 Transverse jets and their control. Prog. Energy Combust. Sci. 36, 531-553.
- MEGERIAN, S., DAVITIAN, J., ALVES, L. S. DE B. & KARAGOZIAN, A. R. 2007 Transverse-jet shear-layer instabilities. Part 1. Experimental studies. *J. Fluid Mech.* **593**, 93–129.
- MEYER, K. E., PEDERSEN, J. M. & ÖZCAN, O. 2007 A turbulent jet in crossflow analysed with proper orthogonal decomposition. *J. Fluid Mech.* **583**, 199–227.
- PAVITHRAN, S. & REDEKOPP, L. G. 1989 The absolute-convective transition in subsonic mixing layers. *Phys. Fluids* A 1, 1736–1739.
- PEPLINSKI, A., SCHLATTER, P. & HENNINGSON, D. S. 2015 Global stability and optimal perturbation for a jet in cross-flow. *Eur. J. Mech* (B/Fluids) **49**, 438–447.
- POLING, B. E., PRAUSNITZ, J. M. & O'CONNELL, J. P. 2001 The Properties of Gases and Liquids, 5th edn. McGraw-Hill.
- REGAN, M. A. & MAHESH, K. 2017 Global linear stability analysis of jets in cross-flow. *J. Fluid Mech.* 828, 812–836.
- SHOJI, T. 2017 Mixing and structural characteristics of unforced and forced jets in crossflow. PhD thesis, University of California, Los Angeles.
- STRYKOWSKI, P. J. & NICCUM, D. L. 1991 The stability of countercurrent mixing layers in circular jets. *J. Fluid Mech.* **227**, 309–343.
- STRYKOWSKI, P. J. & NICCUM, D. L. 1992 The influence of velocity and density ratio on the dynamics of spatially developing mixing layers. *Phys. Fluids* A **4** (4), 770–781.